

Cycle-slip-less low complexity phase recovery algorithm for coherent optical receivers

VALERY NOBL ROZENTAL^{1*}, DEMING KONG^{1,2}, BENJAMIN FOO¹, BILL CORCORAN^{1,2}, AND ARTHUR JAMES LOWERY^{1,2}

¹*Electro-Photonics Laboratory, Department of Electrical & Computer Systems Engineering, Monash University, Clayton, VIC, 3800, Australia*

²*Centre for Ultrahigh-bandwidth Devices for Optical Systems (CUDOS), Australia*

**Corresponding author: valery.rozental@monash.edu*

We propose and experimentally validate a blind phase recovery algorithm based on tracking low-frequency components of the phase noise, which we call “filtered carrier-phase estimation (F-CPE)”. Tracking only the low-frequency components allows F-CPE to both reduce the computational complexity by using a frequency-domain equalizer, and to simplify the QPSK partitioning of a 16QAM constellation. Further, this approach eliminates cycle slips by suppressing the impact of ASE on phase noise estimation. Experimental results demonstrate cycle-slip-free operation for 15- and 32-GBd 16QAM signals. Additionally, the proposed method showed similar or better sensitivity compared with the blind-phase-search algorithm, near standard FEC thresholds of modern WDM systems.

OCIS codes: (060.0060) *Fiber optics and optical communications;* (060.1660) *Coherent communications.*

Carrier phase estimation (CPE) in coherent optical receivers continues to attract researchers’ attention due to migration from QPSK to higher modulation formats for 400G transmission, and increased performance requirements under soft-decision forward error correction (FEC) ([1–3]). An additional motivation is the high computational complexity of the blind-phase-search (BPS) [4], which is considered to be a benchmark algorithm for high-order modulation formats [1] by virtue of its convenient implementation in hardware.

Laser phase noise is commonly modeled as a discrete-time Wiener process with normally-distributed incremental phase $\Delta\theta = \theta_{k+1} - \theta_k$; $\Delta\theta \sim \mathcal{N}(0, 2\pi\Delta\nu T_s)$, where $\Delta\nu$ is the sum of carrier and local oscillator laser linewidths, and T_s is the sampling interval [5]. Usually, CPE is implemented as an all-feedforward structure, because the feedback computation’s latency would increase $\Delta\theta$ ’s variance [6]. For QPSK, the most renowned feed-forward algorithm is Viterbi & Viterbi (V&V) [7], where the noisy constellation is raised to the 4th-power to remove modulated information, collapsing the QPSK constellation around a single point, followed by argument extraction over an averaging window for noise reduction. Naturally, this averaging is suboptimal, because it does not take into account the temporal correlation

of the phase noise, nor the ratio between phase and additive noise components. A two-stage algorithm, which approximates a *maximum a posteriori* (MAP) estimator, was proposed in [5], in which the phase is estimated by V&V, followed by a Wiener filter. It was shown that ideal filter coefficients consist of pre- and post-cursor symmetric exponentially decaying sequences. Alternatively, in [8] a Wiener filter is applied to the 4th-power-raised symbols prior to phase extraction. For 16QAM, raising to 4th-power does not remove all the information, and so QPSK partitioning was proposed in [9, 10], where symbols of the inner and outer radii are treated as QPSK, and the symbols of the central radius are treated as two rotated QPSK sets, which increases complexity by requiring additional decision and de-rotation operations. In [11], the authors used a sliding window to smooth the extracted phase, as opposed to the block-by-block estimation in [10], where a single phase estimate is applied to the whole block. Additional phase recovery techniques, based on Kalman filters, have also been proposed [12, 13].

One drawback of blind-phase-estimation schemes is that they are insensitive to 90-degree phase rotations, which can lead to cycle slips — phase discontinuities of multiples of $\pi/2$, induced by the phase unwrapping operation [5] — especially under low optical signal to noise ratio (OSNR) conditions. One way to deal with cycle slips is by using differential decoding, however, this yields a bit error rate (BER) penalty. At high OSNRs, differential decoding doubles the BER for QPSK, and increases it by $1.65\times$ for 16QAM. Several techniques have been proposed to mitigate cycle slips. In [14, 15], the authors rely on pilot symbols, which has the drawback of reducing spectral efficiency. Alternatively, in [16], cycle slips are treated within the decoder block. Another cycle slip detection and correction scheme was proposed in [17] as an add-on to a generic phase search. Clearly, these techniques further increase processing complexity.

In this letter we argue that, rather than attempting to effectively estimate phase noise, in practical scenarios it is sufficient to track only its low-frequency components, obtained by aggressive low-pass (LP) filtering (order of several MHz). We present and validate an efficient algorithm for low-frequency carrier phase-noise estimation — filtered-CPE (F-CPE) — based on simplified QPSK partitioning, raising to 4th-power, and frequency-domain LP filtering. Although filtering is extensively used in CPE algorithms (e.g., V&V and BPS use averaging windows; the scheme in [11] uses sliding window; in [2], filtering mitigates quanti-

zation noise), the key difference is that we apply LP filtering *before* phase extraction, which leads to an extreme resilience to additive noise, and cycle slip elimination. Experimental results show that F-CPE either outperforms, or has similar performance to BPS, for pre-FEC BER values that comprise modern hard- and soft-decision coding schemes for dense wavelength division multiplexing (DWDM) systems.

Filtered-CPE: The block diagram of the proposed algorithm is depicted in Fig. 1. It is applied after dynamic equalization and frequency offset compensation, at one-sample-per-symbol. F-CPE consists of QPSK partitioning, raising to the 4th power, frequency-domain aggressive low-pass filtering, argument extraction (divided by 4), and phase unwrapping. In the following, we describe the individual F-CPE blocks.

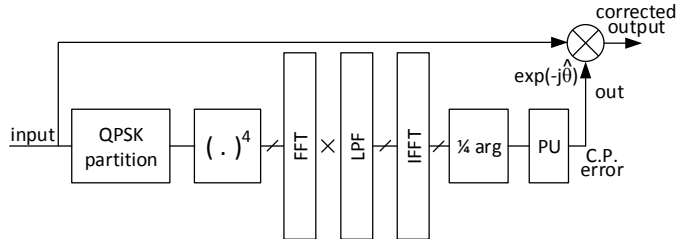


Fig. 1. Filtered CPE block diagram. (I)FFT - (inverse) fast Fourier transform, LPF - low-pass filter, PU - phase unwrapper.

We propose a simplified QPSK partitioning. We begin by considering exclusively the outer ring 16QAM symbols, which form a QPSK constellation. The outer ring symbols are the most distant from the origin, and so offer the best phase noise to amplified spontaneous emission (ASE) ratio. That is, for the same ASE noise, the phase noise is most easily discernible for the outer constellation points. Further, to avoid noise-induced decision errors, we set the partition threshold higher than the usual decoding decision threshold, as shown in Fig. 2(a). The decision threshold for a normalized to unitary power 16QAM constellation is ~ 1.17 . In this work, we arbitrarily set the partition threshold to 1.2, though, further multi-variable optimization for threshold *vs.* OSNR *vs.* $\Delta\nu T_s$ is possible. All symbols below the threshold are set to zero. The resulting constellation is shown in Fig. 2(b).

At one sample-per-symbol, the signal produces a flat spectrum across the digitally-defined frequencies. To extract the carrier information, the 4th-power operation is required. Figs. 2(c-d) show the power spectrum of the QPSK-partitioned signal in Fig. 2(b) before and after raising to the 4th-power. For the experimental setup described hereafter, the bandwidth of the carrier after the 4th-power operation is ~ 15 -20 MHz (see inset Fig. 2(d)), relating to carrier bandwidth of ~ 3 MHz (Fig. 4(b)). Intuitively, this is because phase transitions after raising to the 4th-power occur four times faster.

The low-frequency carrier information is extracted by low-pass filtering (LPF). For finite impulse response (FIR) structures, low-pass filtering can be efficiently applied in the frequency domain using long data sequences filtering algorithms, such as overlap-&-save and overlap-&-add [18]. Finally, the quartered argument (*i.e.*, $1/4$ arg) is extracted from the filtered signal and phase-unwrapped before phase noise compensation. The phase unwrapping is required because of the $1/4$ arg operation, which maps arguments from the $[0, 2\pi]$ interval to $[-\pi/4, \pi/4]$. Thus, F-CPE provides a twofold noise rejection — first through the specific QPSK partitioning, and second, through aggressive filtering prior to argument extraction — resulting in excellent robustness

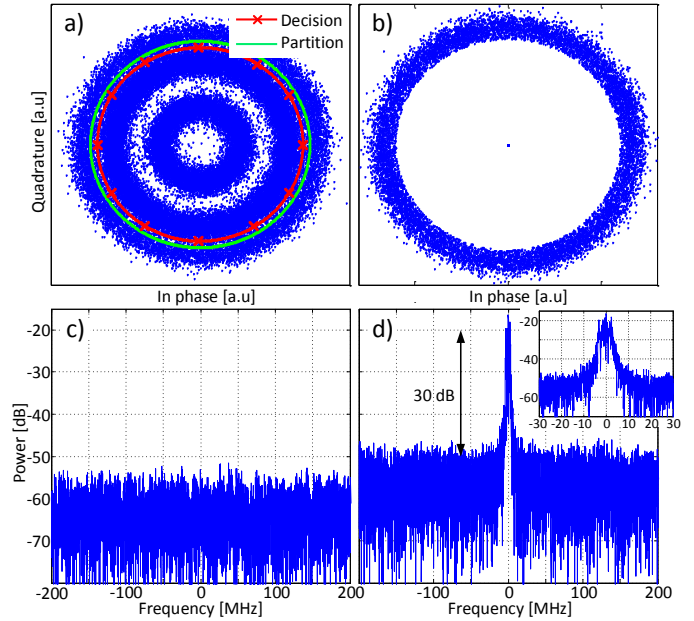


Fig. 2. Proposed simplified QPSK partitioning: (a) threshold setting; (b) resulting constellation; (c) power spectrum of the signal in (b); (d) power spectrum of the signal in (b) raised to the 4th-power. Inset: enhanced resolution around carrier bandwidth.

against cycle slips.

Experimental setup: Correct detection of cycle slips in digital domain usually requires complex signal processing [19, 20] and is not immune to errors. Therefore, the experimental setup, depicted in Fig. 3, is designed to detect cycle slips without signal processing. It produces a noisy signal in one polarization (for reference, X-pol), and maintains an unimpaired, unmodulated carrier in the orthogonal polarization (Y-pol), so that we can unambiguously detect cycle slips by comparing the phases of X- and Y-pols. The transmit-side includes a 92-GSa/s arbitrary waveform generator (AWG) with 32-GHz bandwidth and 8-bit resolution, whose outputs generate in-phase and quadrature components of a single-polarization Nyquist (raised cosine, roll-off 0.2) 16QAM signal. Amplified AWG outputs drive one polarization of a 35-GHz InP dual-polarization modulator. The continuous wave source is an external-cavity laser (Alnair TLG-300-C-4-PM) with a <100 -kHz linewidth. The second polarization remains unmodulated. To generate ASE noise, we used two cascaded erbium-doped fiber amplifiers (EDFAs) with a 100-GHz optical filter between them. Next, the ASE is polarized by a polarization beam splitter (PBS1), and combined with the signal in X-pol by aligning two polarization controllers (Pol Ctrl1 and Pol Ctrl2) with the polarization beam splitter PBS2 (later removed from the setup). Controller PBS3 aligns the signal and the carrier to the receiver polarization axes, and the signal is pre-filtered, and detected by a 25-GHz bandwidth integrated coherent receiver with <100 -kHz linewidth external-cavity laser local oscillator (Agilent N7714A). Finally, the electrical signal in both polarizations is sampled at 80 GSa/s by a real-time scope for digital signal processing, which includes Gram-Schmidt orthonormalization, a radius-directed blind equalizer, and frequency offset compensation [21].

In this setup, OSNR values do not offer intuitive insight into signal quality. As such, we adopt the Q factor as the signal quality metric. Q is estimated directly from the dynamic equalizer output, prior to carrier recovery, as:

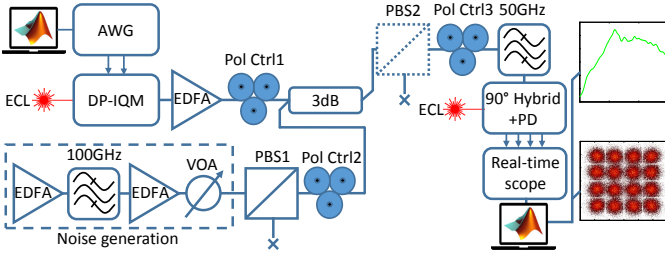


Fig. 3. Experimental setup. AWG—arbitrary waveform generator; ECL—external cavity laser; EDFA—erbium-doped fiber amplifier; DP-IQM—dual pol. IQ modulator; PBS—polarization beam splitter; Pol Ctrl—polarization controller; VOA—variable optical attenuator; PD—photodetector diode.

$$Q[\text{dB}] = 10 \log_{10} \left(\frac{\sum_{n=1}^N |s_n|^2}{\sum_{n=1}^N (|y_n| - |s_n|)^2} \right) - 3, \quad (1)$$

where y_n is the vector of constellation points after DE, and s_n is the vector of transmitted symbols. A -3 dB offset accounts for computing the errors as absolute values rather than in bi-dimensional space. This strategy avoids counting in constellation distortion by phase search algorithms at low SNR.

The phase reference for cycle slip detection is extracted from the digitized samples of Y-pol as follows. First, frequency offset (in both polarizations) is coarsely compensated by shifting the carrier peak to zero frequency, as shown in Fig. 4(a). Next, a 3-MHz low-pass filter (10^{th} -order super-Gaussian) is applied to extract the carrier component, as shown in Fig. 4(b). The resulting signal is downsampled to 1 sample-per-symbol, and argument is extracted.

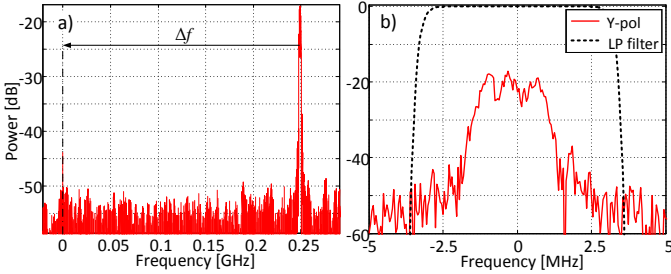


Fig. 4. (a) Coarse frequency offset compensation; (b) Carrier spectrum (high resolution) and phase extractor filter.

Results and discussion: We assess two symbol rates, $R_s = 15$ and 32 GBd, targeting 100 and 200 Gb/s transmission, which yields $\Delta\nu T_s = 1.33 \times 10^{-5}$ and $\Delta\nu T_s = 6.25 \times 10^{-6}$, respectively. The performance is evaluated under two separate criteria: (i) sensitivity, and (ii) cycle slip occurrences. As a performance reference, we use the BPS algorithm, which has two adjustable parameters: the number of test carrier phases (B) and the number of samples in the averaging window (W) [4]. We compare the performance of F-CPE against two BPS configurations: a practical case configuration ($B = 20, W = 20$), and an “ideal” configuration ($B = 200^2, W = 100$). The $B = 200^2$ notation refers to BPS, where in the first stage we conduct a coarse phase search with $B = 200$, and in the second stage we conduct a fine search around the phase value found in the first stage, resulting in phase granularity of $90/200^2 = 2.2 \times 10^{-3}$ degrees.

For F-CPE low-pass filtering, we design a Hamming-windowed FIR filter, with a 20-MHz 3-dB cutoff frequency, following the results in Fig. 2(d). The corresponding frequencies, normalized to half the sampling rate (*i.e.*, normalized to $R_s/2$)

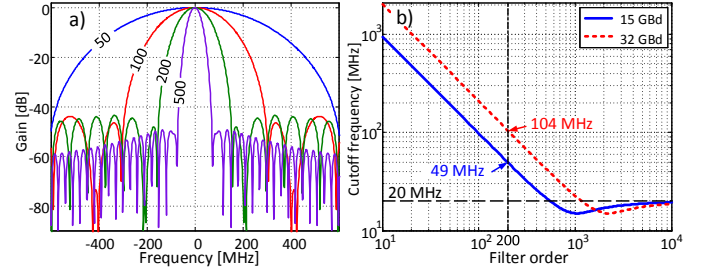


Fig. 5. (a) Frequency response for selected filter orders (15 GBd); (b) true 3-dB cutoff frequency *vs.* LPF order (design 3-dB frequency is 20 MHz).

are 2.7×10^{-3} , and 1.3×10^{-3} for 15- and 32-GBd signals, respectively. In general, such low cutoff frequencies require very long FIR structures. This can be observed in Fig. 5(a), which shows the LPF frequency response for selected filter orders (filter order = number of taps - 1), designed for a 15-GBd signal. As the filter order increases, the cutoff frequency approximates the desired value. Fig. 5(b) plots the actual cutoff frequencies as a function of filter order (log.-log. scale). In our implementation, the cutoff frequency stabilizes at 20 MHz only when FIR length is $\sim 10,000$ taps. However, as we will show in the following, much smaller filters achieve satisfying performance.

We first compare F-CPE and BPS sensitivities in terms of BER for selected Q values. Differential decoding is used for BER count to eliminate the impact of possible cycle-slip-induced error bursts on sensitivity performance. Figs. 6(a-b) show the obtained results for 15- and 32-GBd signals. Traces that correspond to F-CPE are plotted against the LPF order, where each trace represents an average of five independent data captures. Filtering was implemented in the frequency domain using overlap-&-save method with FFT size 2^{13} . The BPS performance for “ideal” and practical cases is indicated by solid and dashed horizontal black lines. At 15 GBd, F-CPE outperforms BPS for all the selected Q values when FIR filter order is above 150. At 32 GBd, the F-CPE performance is quasi-identical to the “ideal” BPS for BER $> 10^{-2}$ and filter order above 200, and identical to the practical case BPS for BER $\sim 10^{-3}$. For BER $\sim 10^{-4}$, F-CPE roughly doubles the number of errors with respect to BPS. However, these BER values are considerably below common DWDM hard-decision FEC limits (*i.e.*, BER $> 10^{-3}$) [22]. Increasing the LPF order above 200 produces only marginal improvement for both symbol rates, and so in the rest of this letter we use 200th-order filters, whose true cutoff frequencies are 49 and 104 MHz for 15 and 32 GBd (see Fig. 5(b)). It is worth noting that FIR filter order has a direct

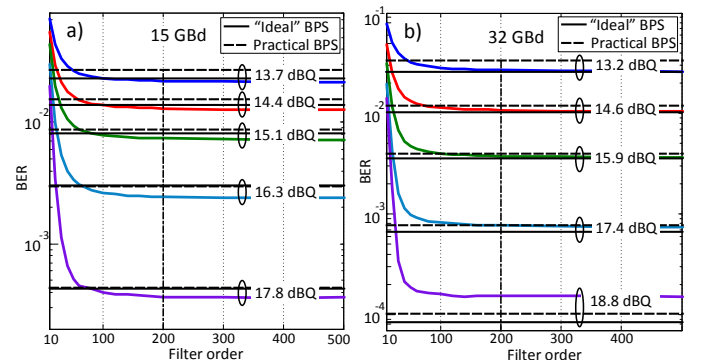


Fig. 6. F-CPE sensitivity results: BER (differential decoding) *vs.* LPF order for selected Q values: (a) 15 GBd; (b) 32 GBd.

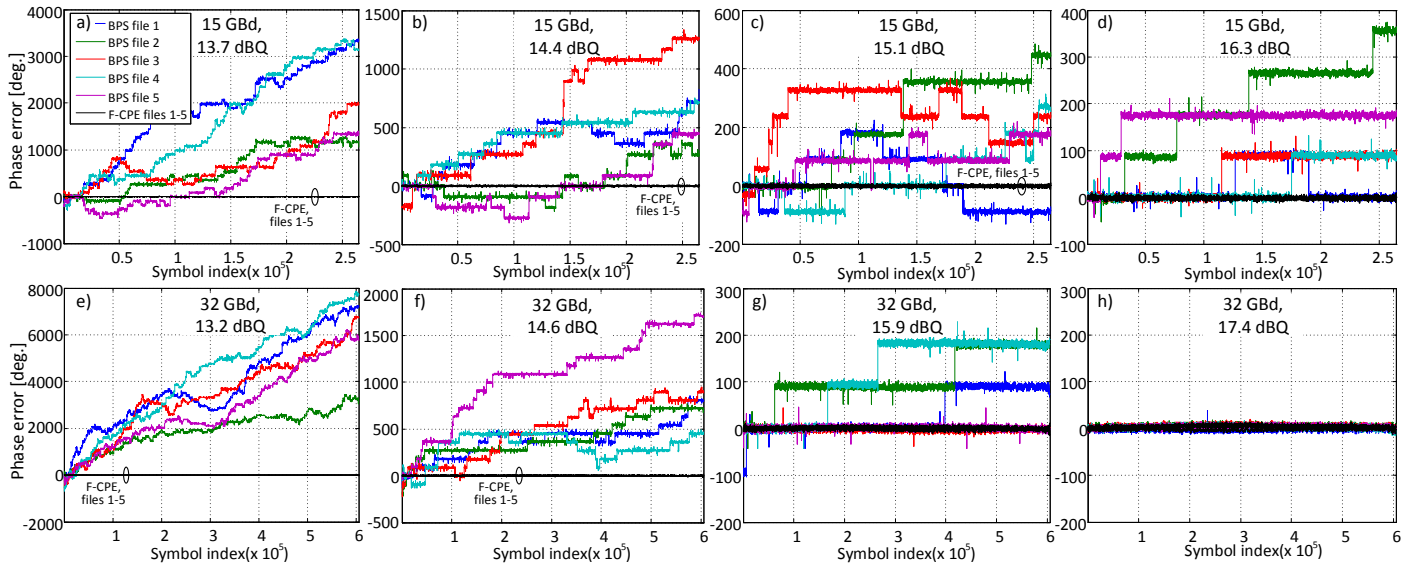


Fig. 7. Phase errors for F-CPE and practical case BPS. (a-d) 15 GBd; (e-h) 32 GBd. Colored traces: BPS phase errors; Black traces (overlapped): F-CPE phase errors.

impact on computational complexity, because it represents the minimum overlap size of long data filtering algorithms (*i.e.*, the FFT portion that does not produce useful data).

Finally, we evaluate the robustness of F-CPE against cycle slips, comparing its performance to the practical case BPS ($B = 20$, $W = 20$). Figs. 7(a-h) show the obtained results. Each figure shows errors between the phase values estimated by F-CPE and BPS, and phase values extracted from Y-pol, for selected Q values. The traces in each figure indicate five independent captures, where upper-row figures (Figs. 7(a-d)) correspond to 15 GBd, and lower-row figures (Figs. 7(e-h)) correspond to 32 GBd. The colored traces indicate BPS, and the black traces (overlapped) indicate F-CPE. Cycle slips are clearly observed for BPS, producing $\pm 90^\circ$ phase error jumps. Conversely, F-CPE did not present any cycle slips under the tested scenarios.

In summary, we have proposed and experimentally validated a novel blind phase recovery algorithm. F-CPE is based on low-frequency phase component estimation, and has two noise rejection mechanisms: simplified QPSK partitioning and MHz-range low-pass filtering, which makes it immune to cycle slips. In addition, being based on frequency-domain filtering, its complexity is greatly reduced in comparison with BPS. Experimental results of a 16QAM transmission show that F-CPE either outperforms, or shows similar sensitivity to BPS, for signal quality comparable with the modern DWDM forward error correction codes.

Funding. The Australian Research Council's – ARC Laureate Fellowship (FL130100041); CUDOS – ARC Centre of Excellence for Ultra-high Bandwidth Devices for Optical Systems (CE110001018).

REFERENCES

1. M. S. Llopis, M. S. Faruk, and S. J. Savory, in *Optical Fiber Communication Conference*, (Optical Society of America, 2017), paper Th4C.2.
2. J. Rodrigo Navarro, A. Kakkar, R. Schatz, X. Pang, O. Ozolins, A. Udalcovs, S. Popov, and G. Jacobsen, *Photonics* **4** (2017).
3. C. Zhu and N. Kaneda, in *Optical Fiber Communication Conference*, (Optical Society of America, 2017), paper Th4C.1.
4. T. Pfau, S. Hoffmann, and R. Noe, *J. Lightwave Technol.* **27**, 989 (2009).
5. E. Ip and J. M. Kahn, *J. Lightwave Technol.* **25**, 2675 (2007).
6. M. G. Taylor, *J. Lightwave Technol.* **27**, 901 (2009).

7. A. Viterbi and A. Viterbi, *IEEE Trans. Inf. Theory* **29**, 543 (1983).
8. F. A. Garcia, D. A. Mello, and H. Waldman, *Opt. Express* **17**, 7958 (2009).
9. H. Louchet, K. Kuzmin, and A. Richter, in *European Conference on Optical Communication*, (2008), paper Tu.1.E6.
10. I. Fatadin, D. Ives, and S. J. Savory, *IEEE Photon. Technol. Lett.* **22**, 631 (2010).
11. I. Fatadin, D. Ives, and S. J. Savory, *IEEE Photon. Technol. Lett.* **26**, 854 (2014).
12. T. Inoue and S. Namiki, *Opt. Express* **22**, 15376 (2014).
13. J. Jignesh, B. Corcoran, and A. Lowery, *Opt. Lett.* **41**, 3253 (2016).
14. H. Zhang, Y. Cai, D. G. Foursa, and A. N. Pilipetskii, in *Optical Fiber Communication Conference*, (Optical Society of America, 2011), paper OMJ.7.
15. L. Liu and L. Li, in *Optical Fiber Communication Conference*, (Optical Society of America, 2014), paper Th4D.2.
16. T. Koike-Akino, K. Kojima, D. S. Millar, K. Parsons, Y. Miyata, W. Matsumoto, T. Sugihara, and T. Mizuochi, in *Optical Fiber Communication Conference*, (Optical Society of America, 2014), paper M3A.3.
17. Y. Gao, E. Ha, A. P. T. Lau, C. Lu, X. Xu, and L. Li, *Opt. Express* **22**, 31167 (2014).
18. J. Proakis and D. Manolakis, *Digital signal processing: principles, algorithms, and applications* (Prentice Hall, 1996), 3rd ed.
19. X. Liu, C. Sethumadhavan, T. Pfau, and G. Gavioli, Patent US2015215050 (A1), Alcatel Lucent, (2015).
20. G. Gao, X. Chen, and W. Shieh, *Opt. Express* **20**, 14406 (2012).
21. S. J. Savory, *IEEE J. Sel. Topics Quantum Electron.* **16**, 2120 (2010).
22. R. J. Essiambre, G. Kramer, P. J. Winzer, G. J. Foschini, and B. Goebel, *J. Lightwave Technol.* **28**, 662 (2010).